

**Supplementary Material for
“Precise Relocation and Source Characterization of Two Earthquake Sequences in Yellow
Sea Using Regional *Lg* Wave Observations”**

Jun Yong Park¹, Won-Young Kim², YoungHee Kim^{1*} and Xuzhang Shen³

¹ School of Earth and Environmental Sciences, Seoul National University, 1 Gwanak-ro, Gwanak-gu, Seoul 08826, Republic of Korea

² Lamont-Doherty Earth Observatory of Columbia University, 61 Route 9W, Palisades, NY 10964, USA

³ Guangdong Provincial Key Lab of Geodynamics and Geohazards, School of Earth Sciences and Engineering, Sun Yat-Sen University, Guangzhou 510275, China

Corresponding author: YoungHee Kim, younghkim@snu.ac.kr

Contents

This supplemental material contains additional details of the seismic data processing and analyses described in text with 11 figures and one table.

Texts

Text S1. Screening outliers of the *Lg* wave cross-correlation measurements.

Figures

Figure S1. Map showing seismographic stations used in this study.

Figure S2. Theoretical travel time curve, observed travel time picks to locate 2021 Gunsan Basin earthquake sequences, and waveform plot showing *Pn* arrivals.

Figure S3. The stations used in regional waveform modeling and focal mechanism inversion.

Figure S4. The waveform modeling and focal mechanism inversion results of the 18 January 2021 mainshock.

Figure S5. Changes of the fitting error and source mechanism as a function of focal depths for the two mainshocks.

Figure S6. Connectivity diagram for the double-difference earthquake relocation using body waves.

Figure S7. Comparison between absolute and relative locations using HYPOINVERSE and hypoDD, respectively.

Figure S8. Differential travel times (dt) for all event pairs using Lg wave cross-correlation with respect to station azimuth.

Figure S9. Observed dt for four event pairs using Lg wave cross-correlation and theoretical sinusoidal curve plotted against station azimuth.

Figure S10. Standard deviation of dt of radial, transverse and vertical components versus distance for four event pairs.

Figure S11. Connectivity of epicentral relocation of event pairs.

Figure S12. Spectral ratio between target (event 1) and EGF (event 5) for all used stations.

Figure S13. Spectral ratio between target (event 7) and EGF (event 8) for all used stations.

Figure S14. Map showing the horizontal projection of the P axis of the mainshock and of 2,204 shallow earthquakes (< 70 km) during 1976 – 2023 around the epicentral region.

Figure S15. Comparison of observed displacement amplitude spectra of Lg wave for events 1 and 7 at nine stations.

Tables

Table S1. Earthquake parameters of the 2021 offshore Gunsan earthquake sequences.

References

Text S1. Screening outliers of the Lg wave cross-correlation measurements

The Lg observations were obtained from over 150 stations around the epicenter at distances between 160 and 550 km (Fig. 1a); the observed differential travel times (dt) from most event pairs show sinusoid with respect to the station azimuth (Figs. 4, S6). We fit the data with the sinusoidal curve using the following equation:

$$dt^{\text{cal}}(\varphi_k) = [\max(dt) + \min(dt)]/2 \times \sin(\varphi_k - \varphi_{12} + 90) + [\max(dt) - \min(dt)]/2 \quad (1)$$

where φ_k denotes the azimuth of k -th station relative to the center of the two events, and φ_{12} the azimuth from event 1 to event 2. The $\max(dt)$ and $\min(dt)$ are the maximum and minimum values of the differential travel time measurements according to station azimuth, respectively. In an ideal case when the differential travel time measurements are evenly distributed with various azimuths, the $[\max(dt)+\min(dt)]/2$ becomes the amplitude of the sinusoid. This amplitude indicates the distance between the two events with a certain velocity, and thus larger amplitudes indicate larger distances. The $[\max(dt) - \min(dt)]/2$ becomes the baseline of the sinusoid which is related to the origin time difference of the two events.

Outlier dt can be screened by using a following criterion: $[dt^{\text{cal}}(\varphi_k) - dt^{\text{obs}}(\varphi_k)] > \pm \sigma/2$, where σ is the standard deviation. In case when the initial location has a large uncertainty and signal-to-noise ratio is low, the threshold can be increased to $\pm \sigma$. The RMS of difference in dt is an indicator of the overall quality of the correlation measurement of the event pair (see Figs. 4, S6). In the DD relocation procedure from the hypoDD code, residual cut and distance cut during the relocation iteration can also effectively screen the outliers.

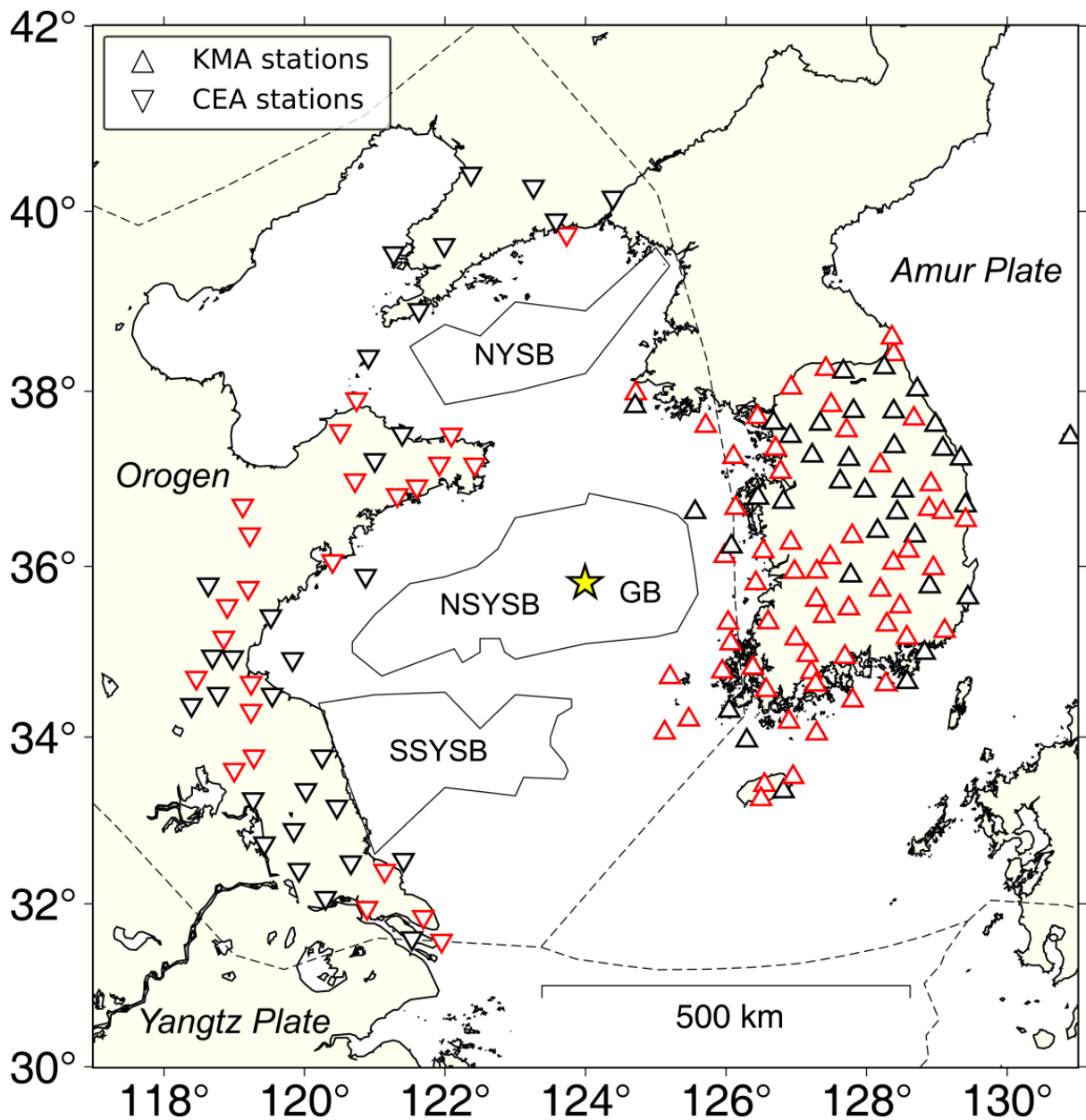


Figure S1. Seismic stations used in this study. A yellow star represents an epicenter of the M_L 4.6 earthquake that occurred on January 18, 2021. Triangles and inverted triangles represent Korea Meteorological Agency (KMA) and China Earthquake Administration (CEA) stations, respectively. Red edged triangles represent stations used in estimating corner frequencies. Dashed and solid black lines represent plate boundaries taken from Bird (2003) and basins, respectively. NYSB = North Yellow Sea Basin; GB = Gunsan Basin; NSYSB = Northern South Yellow Sea Basin; SSYSB = Southern South Yellow Sea Basin.

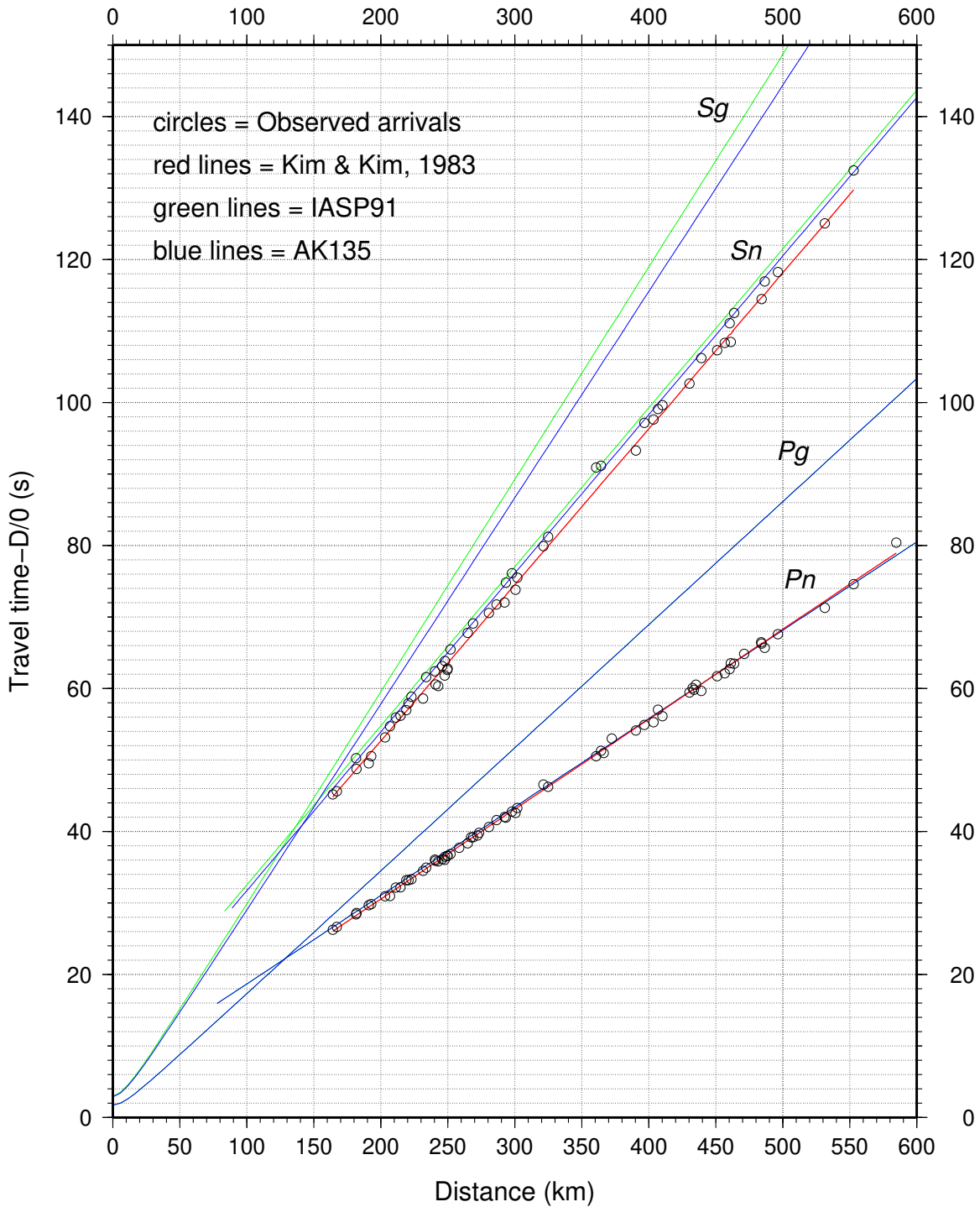


Figure S2a. Observed arrival times of Pn and Sn phases (circles) and corresponding travel times calculated using a two-layer crustal velocity model of Kim and Kim (1983) for a source depth of 10 km that were used in this study (red lines). Travel times calculated from the IASP91 (Kennett and Engdahl, 1991) and AK135 (Kennett et al., 1995) models are plotted for comparison.

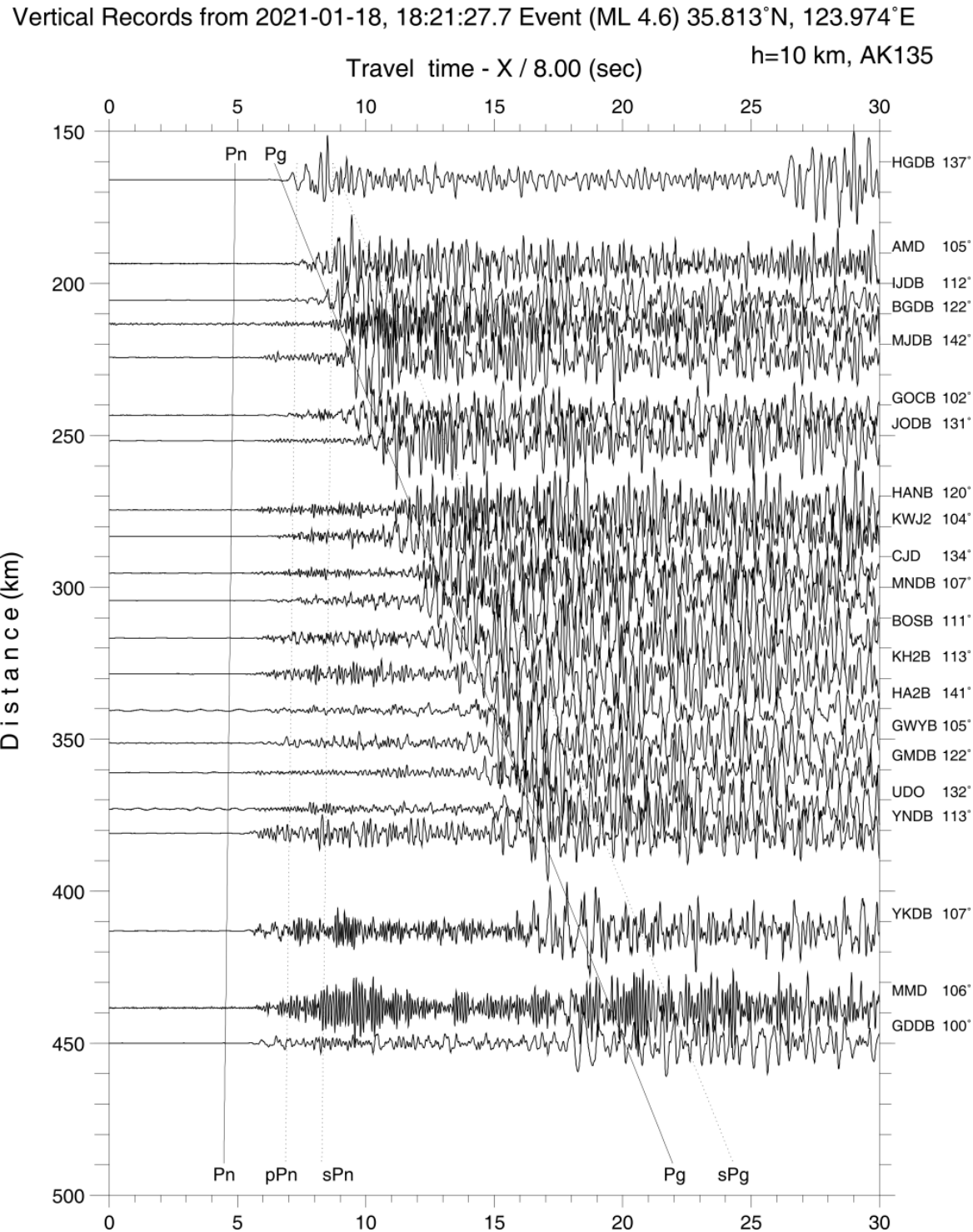


Figure S2b. Waveform plot showing Pn arrivals recorded by KMA stations, as shown in Figure 2a. Selected stations are plotted with a reduced velocity of 8 km/s. Travel times of regional phases calculated with the AK135 crustal model are indicated by black lines. Station names and azimuths are plotted in right-side of each plot.

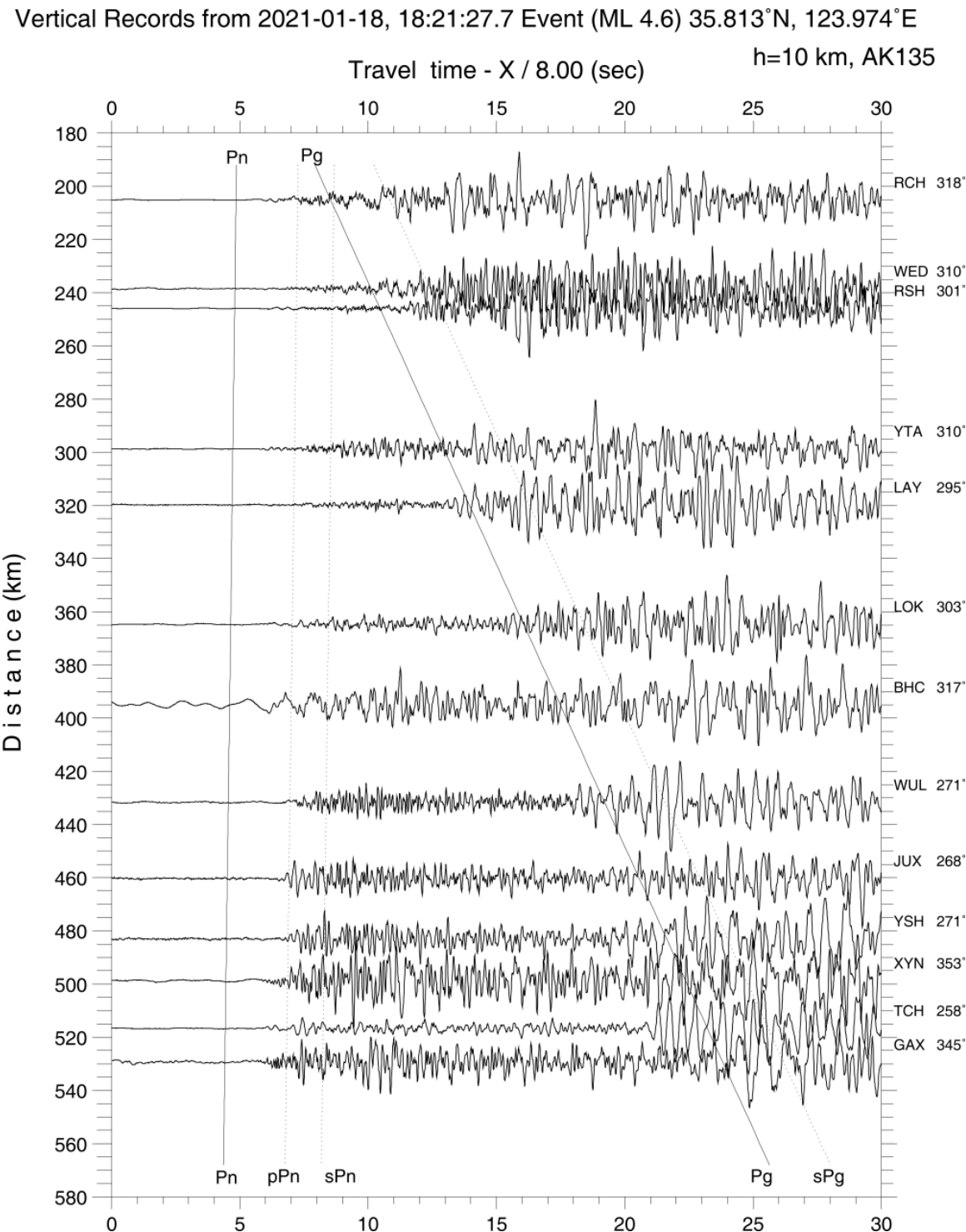


Figure S2c. Waveform plot showing Pn arrivals recorded by CEA stations, as shown in Figure 2b. Others are the same as Figure S2b.

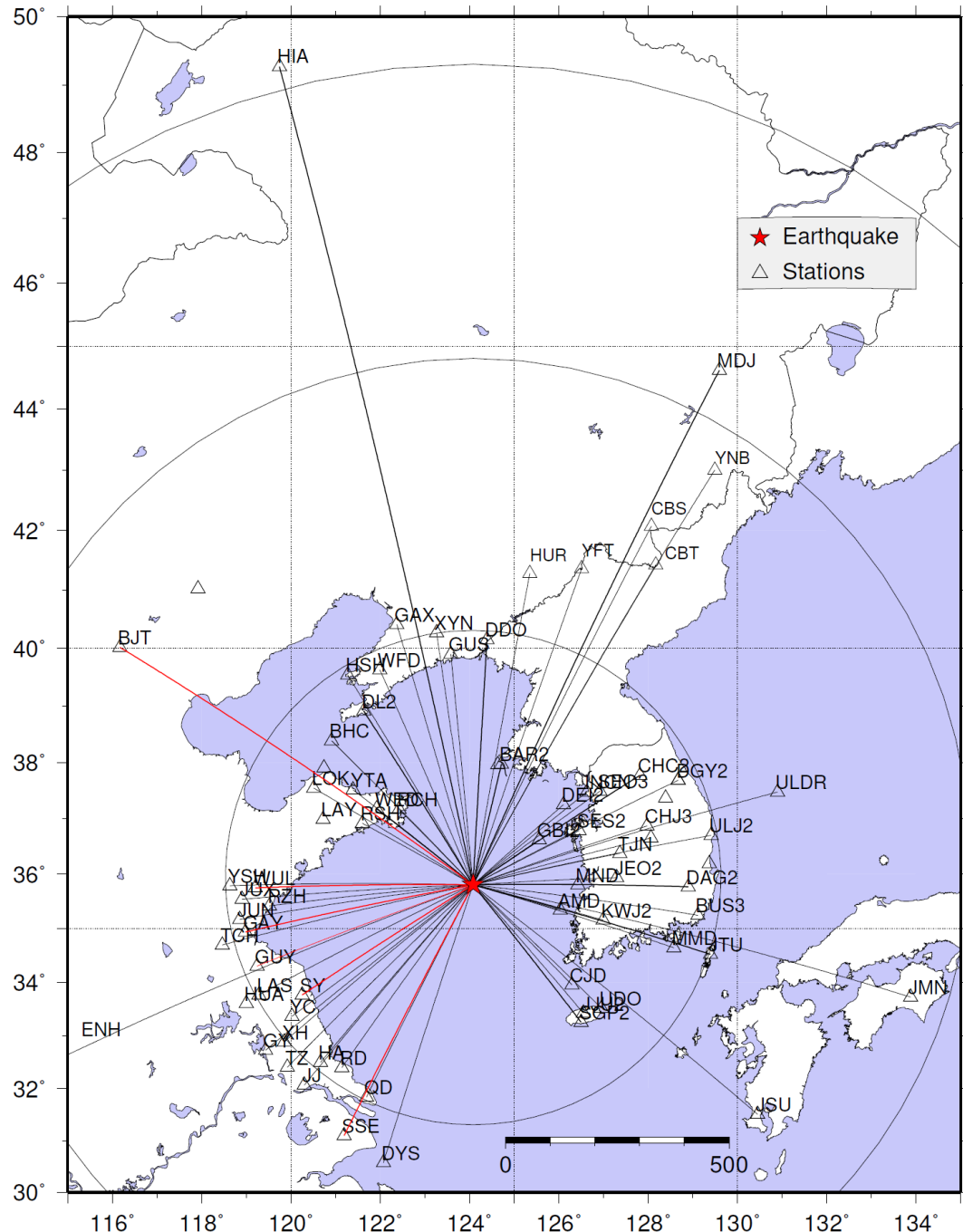


Figure S3. Broadband stations in South Korea, China, and Japan used to analyze the 18 January 2021 Gunsan Basin earthquakes are plotted by triangles; the stations used in regional waveform modeling and focal mechanism inversion are indicated by great circle paths connecting the source-receiver. Red lines indicate stations used to model their long-period records (0.03 – 0.1 Hz) using a two-layer crustal velocity model with a 2-kilometer thick surface low-velocity layer.

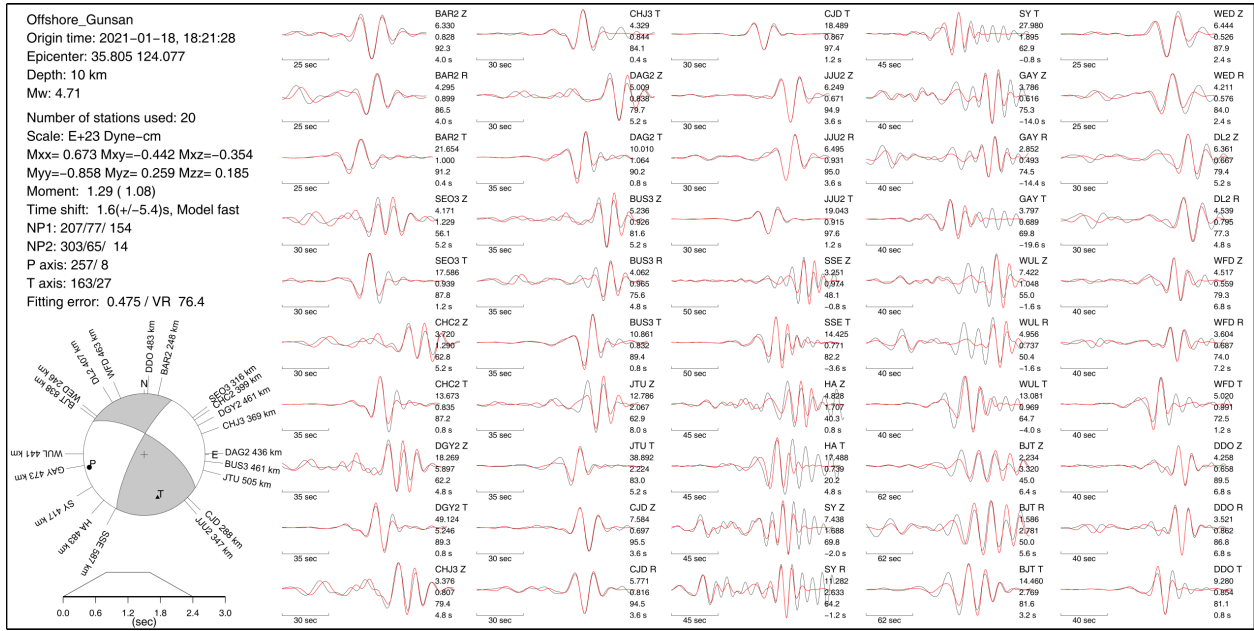


Figure S4. Comparison between observed (black) and synthetic (red) waveforms of the 18 January 2021 mainshock. Synthetic seismograms are calculated for a focal depth of 10 km; 50 traces from 20 stations are shown. Station code, component (Z=vertical, R=radial, T=transverse components), peak amplitude of the observed signal in micrometers, seismic moment in 10^{16} Nm, variance reduction in percent, and time shift δt in second are indicated at the end of each trace. Long-period (10 to 33 s) regional body waves (P_{nl} and S_{nl}) and fundamental mode Rayleigh wave are the main signals. Focal mechanism of the event is represented by the typical beach ball representation of lower-hemisphere projection. Shaded quadrants denote compressional quadrants. The epicentral distance of each station is marked around the beach ball according to azimuth. Two nodal planes (NP1 and NP2), as well as azimuth and plunge angle in degrees of the P and T axes, are indicated. A simple source time function used is shown.

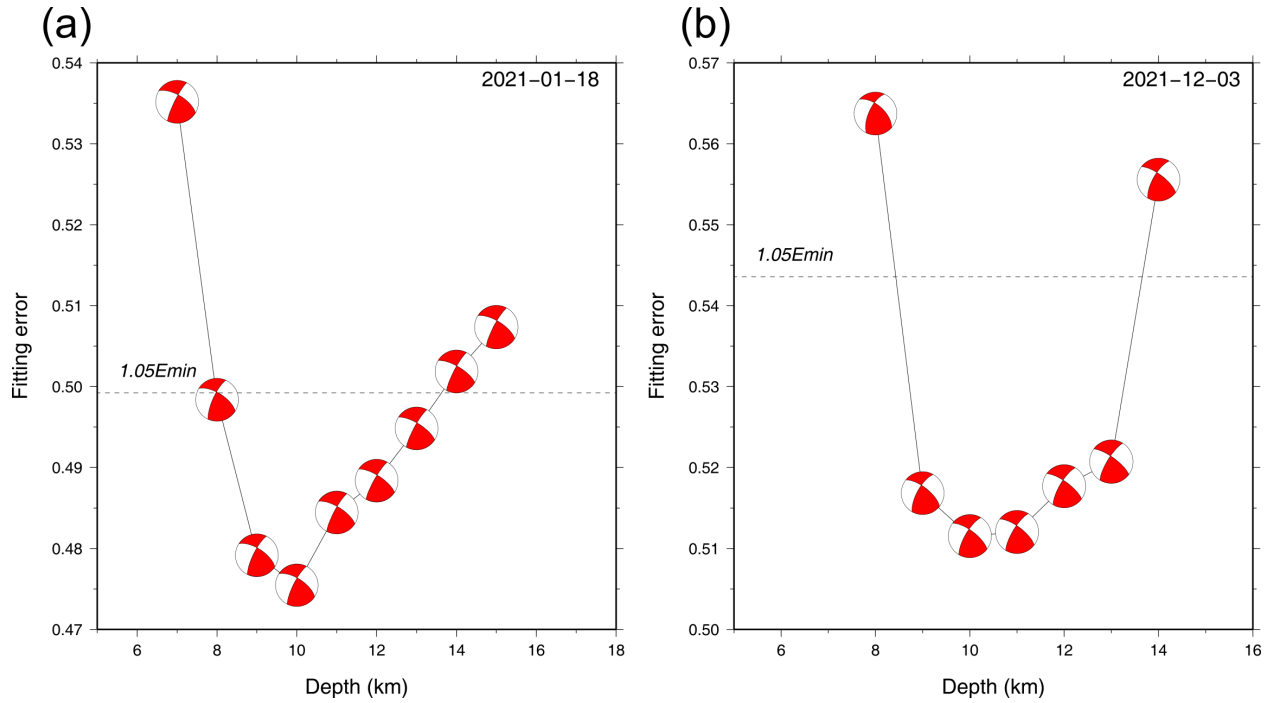


Figure S5. Changes of the fitting error (E) and source mechanism as a function of focal depths for (a) the 18 January and (b) 03 December 2021 mainshocks, respectively. The fitting error reaches a global minimum (E_{min}) at 10 km depth, which is our estimate of the focal depth for the event. The inversion results for focal depths between 8 and 13 km produce similar overall waveform fits as well as source mechanisms, indicating a range of acceptable depths, and are indicated by a horizontal dashed line representing 5% greater fitting error, that is $1.05 \times E_{min}$.

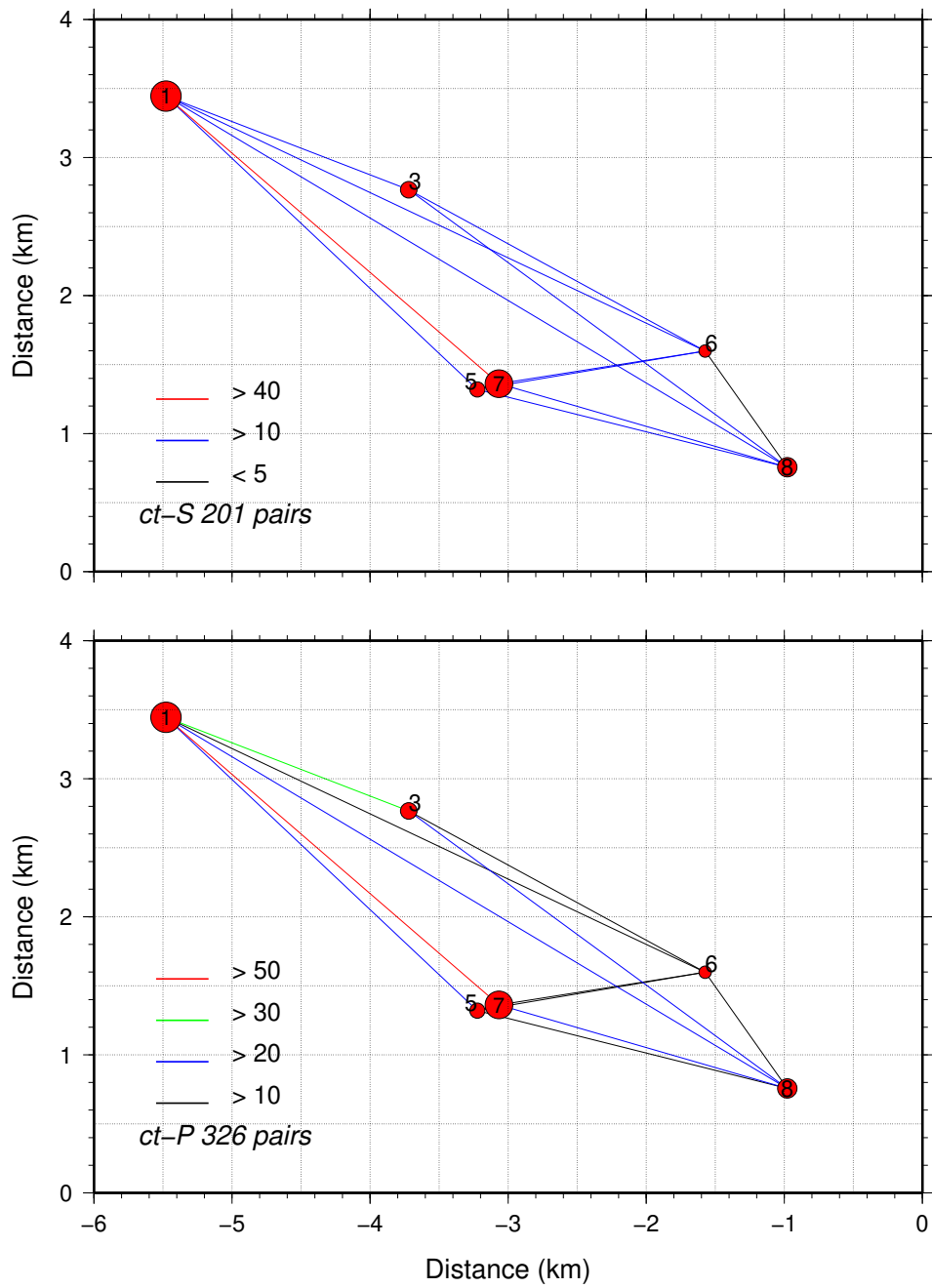


Figure S6. Connectivity diagram for the double-difference earthquake relocation. Final event pair linkages for the relocation are shown. (top) A total of 201 event link pairs for S_n are plotted with a number of observations on each pair (color-coded). (bottom) 326 linkage pairs of the catalog differential data used for the relocation. There are 27 event pairs, so each pair has 12 observations on average. Notice that events 1 and 7 have link pairs with other smaller events.

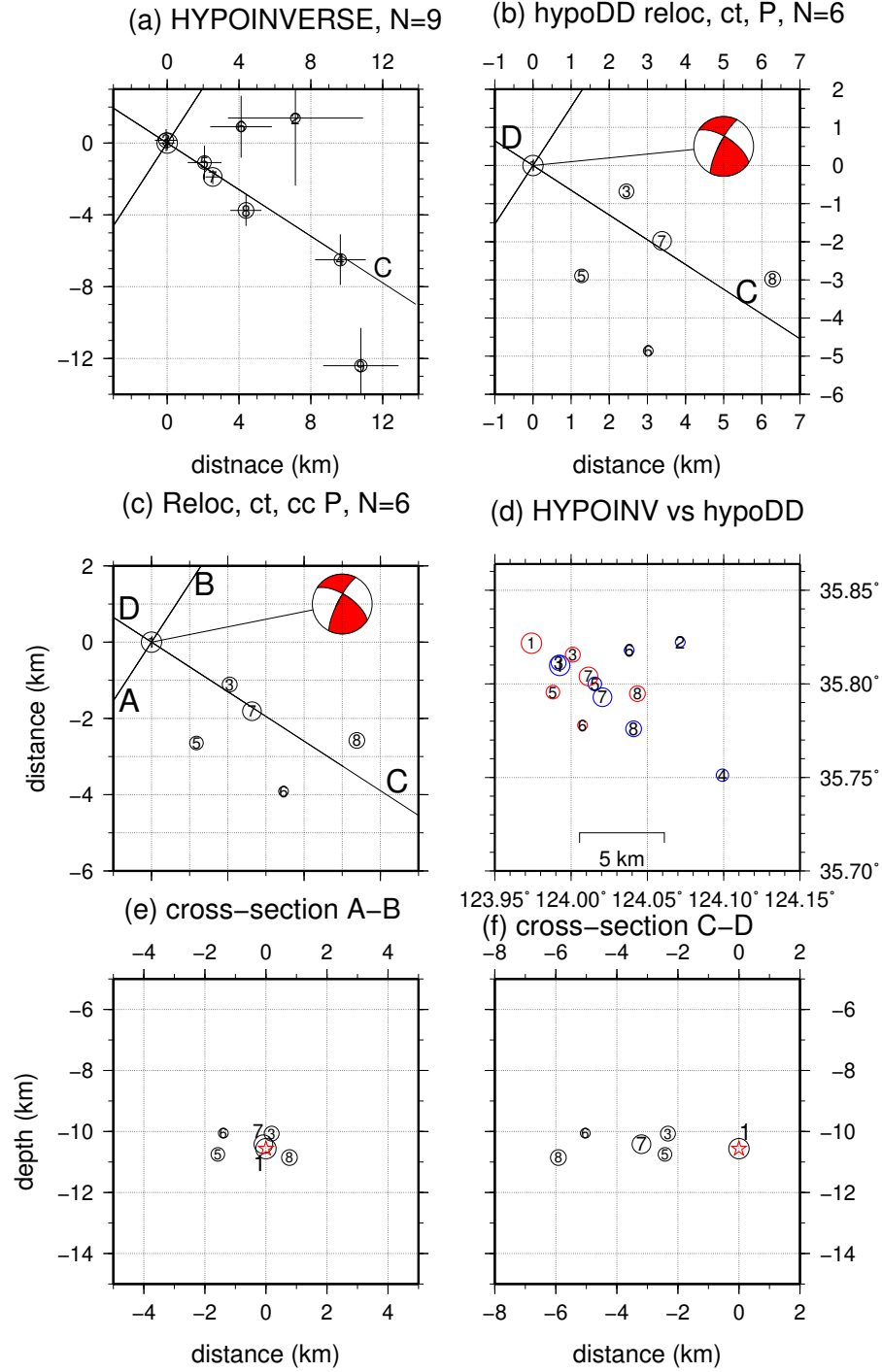


Figure S7. (a) Map-view figure showing nine events located by HYPOINVERSE (Klein, 2002). Notice that events greater than $M > 3$ are located with small location errors (events 1, 3, 5, 7, and 8) and are aligned along the east-southeast (125°) direction. (b) Six events relocated from hypoDD (Waldhauser and Ellsworth, 2000; Waldhauser, 2001) using 608 Pn phase data in 27 event pairs with the maximum interevent separation distance of 3 km during iteration. (c) hypoDD relocation using Pn phase data plus 67 dt from Pn WCC measurements with $Cc > 0.7$.

Few correlation data do not improve the relocation. (d) Comparison of six relocated events in (c) (red circles) and absolute locations of nine events located by using HYPOINVERSE (blue circles). Double-difference relocation improved event locations somewhat, but they can be further improved. (e) across-strike cross-section (A–B) of DD locations using dt values from both phase data and waveform cross-correlation. (f) along strike cross-section (C–D) of DD locations using dt values from the waveform cross-correlation and phase data. A star indicates the mainshock – event 1.

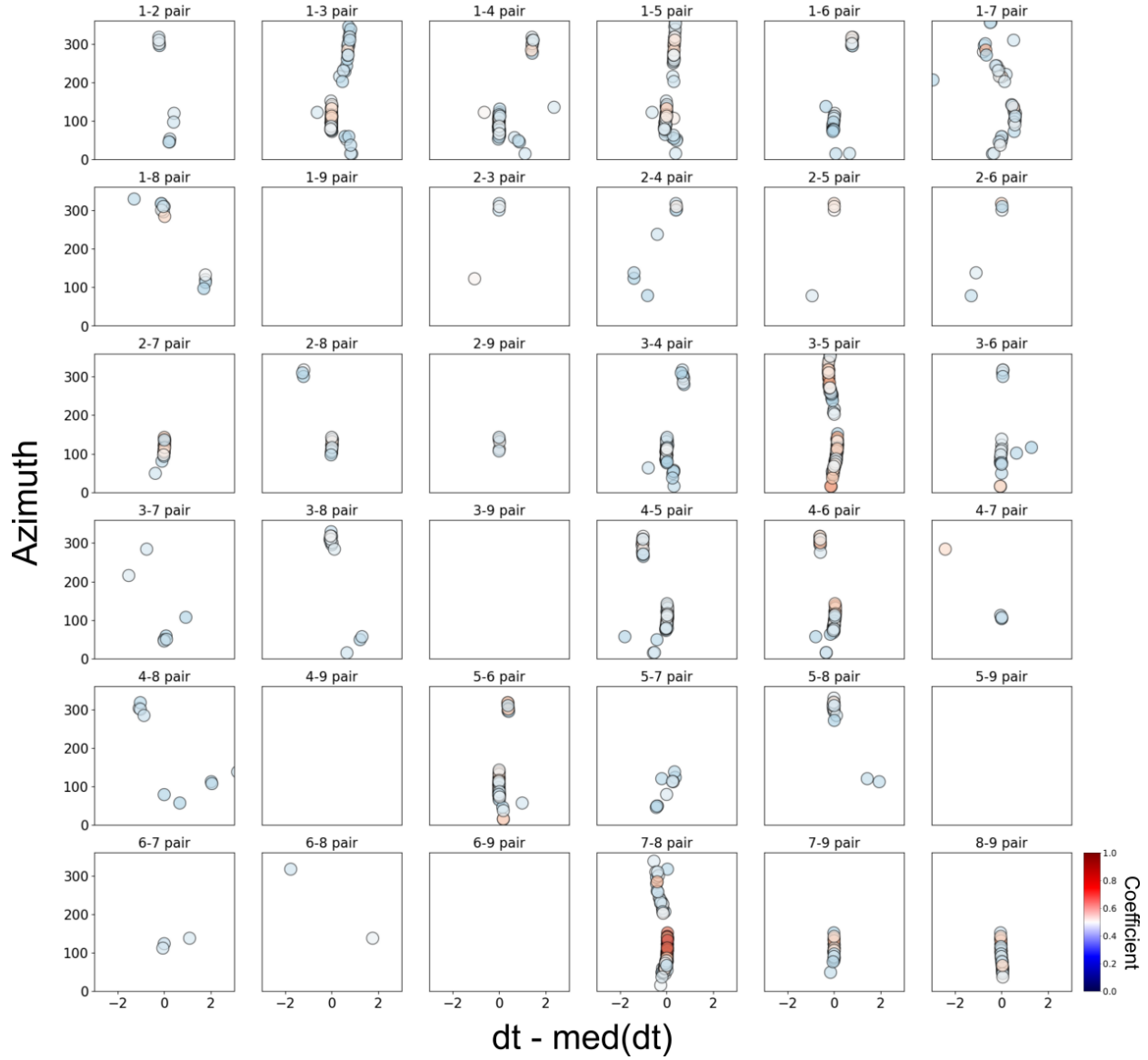


Figure S8. Differential travel times (dt) plotted according to azimuth. Each plot represents each event pair. The color of each circle represents the coefficient. The differential travel times are aligned to each median value.

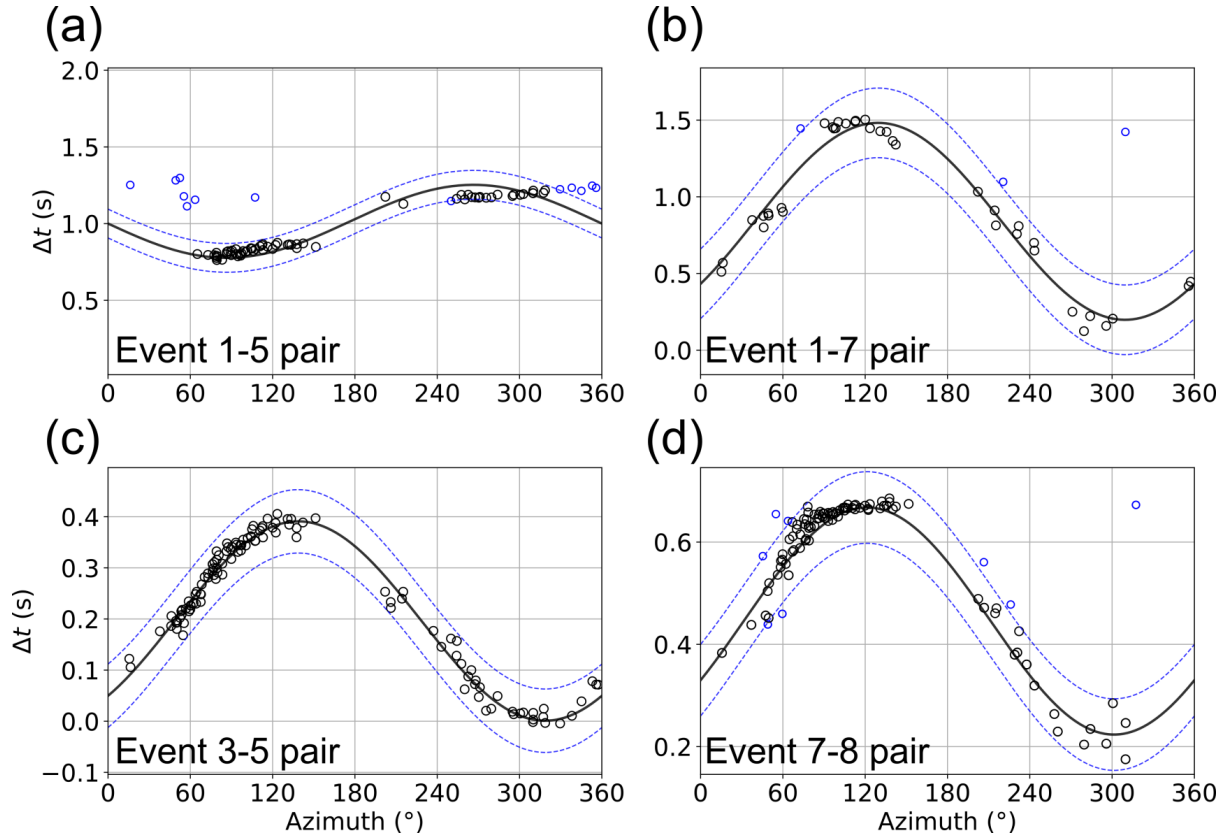


Figure S9. Observed dt for the four event pairs plotted against station azimuth. The dt for a pair of events are expected to show a sinusoid as a function of station azimuth. The distance between the event pair determines the maximum height of the sinusoid, whereas the median or mean of dt is related to the origin time difference. The solid curve represents the calculated sinusoid of station azimuth, and two blue dashed curves represent \pm half standard deviation ($\sigma/2$) of the observed dt . Black and blue circles represent data within $\pm\sigma/2$ and beyond $\pm\sigma/2$, respectively. (a) Event 1–5 pair has an event separation distance of 0.60 km, and the observed dt are distributed around the calculated dt within ± 0.09 s. (b) Event 1–7 pair has an event separation distance of 2.5 km, and the observed dt are distributed around the calculated dt within ± 0.23 s. (c) Event 3–5 pair has an event separation distance of 0.6 km, and the observed dt are distributed around the calculated dt within ± 0.06 s. (d) Event 7–8 pair has an event separation distance of 0.7 km and the observed dt are distributed around the calculated dt within ± 0.07 s.

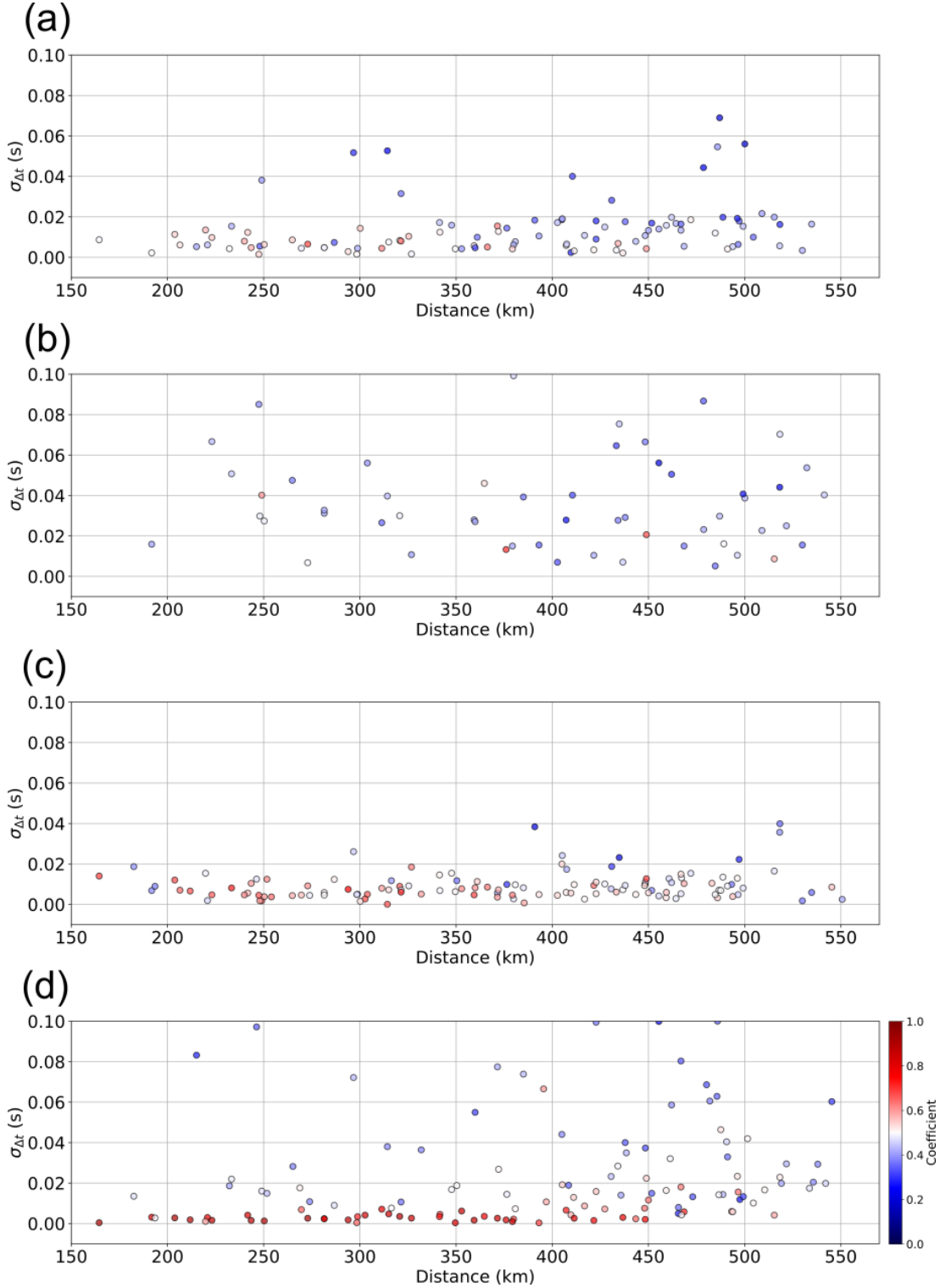


Figure S10. Standard deviation of dt of radial, transverse and vertical components plotted against distance. The color of each circle represent correlation coefficient. (a) Event 1–5 pair. (b) Event 1–7. (c) Event 3–5 pair. (d) Event 7–8.

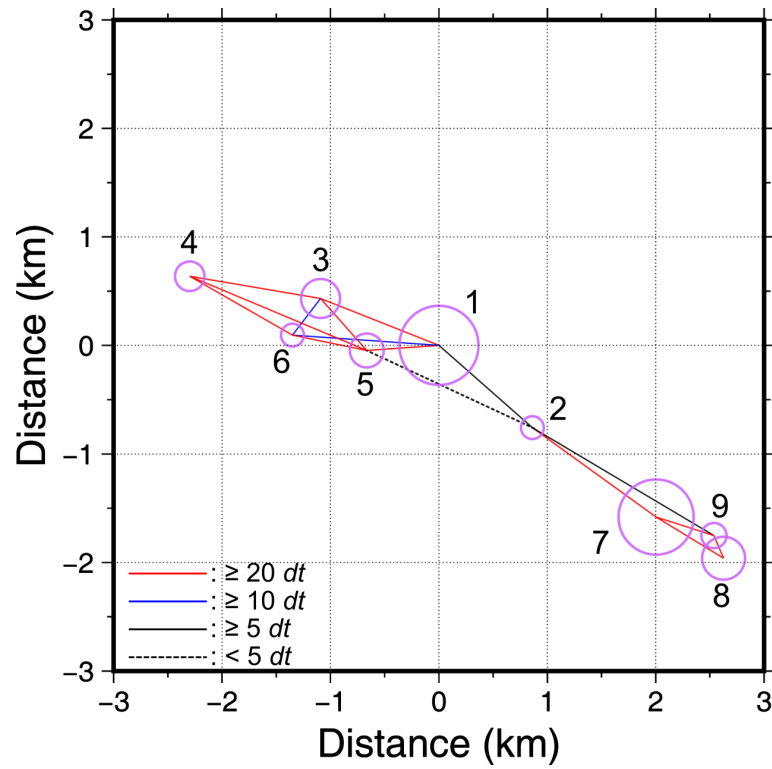


Figure S11. Connectivity of event pairs represented by color coded lines. Total 644 dt from the 16 pairs are used to relocate the events. Event IDs are shown.

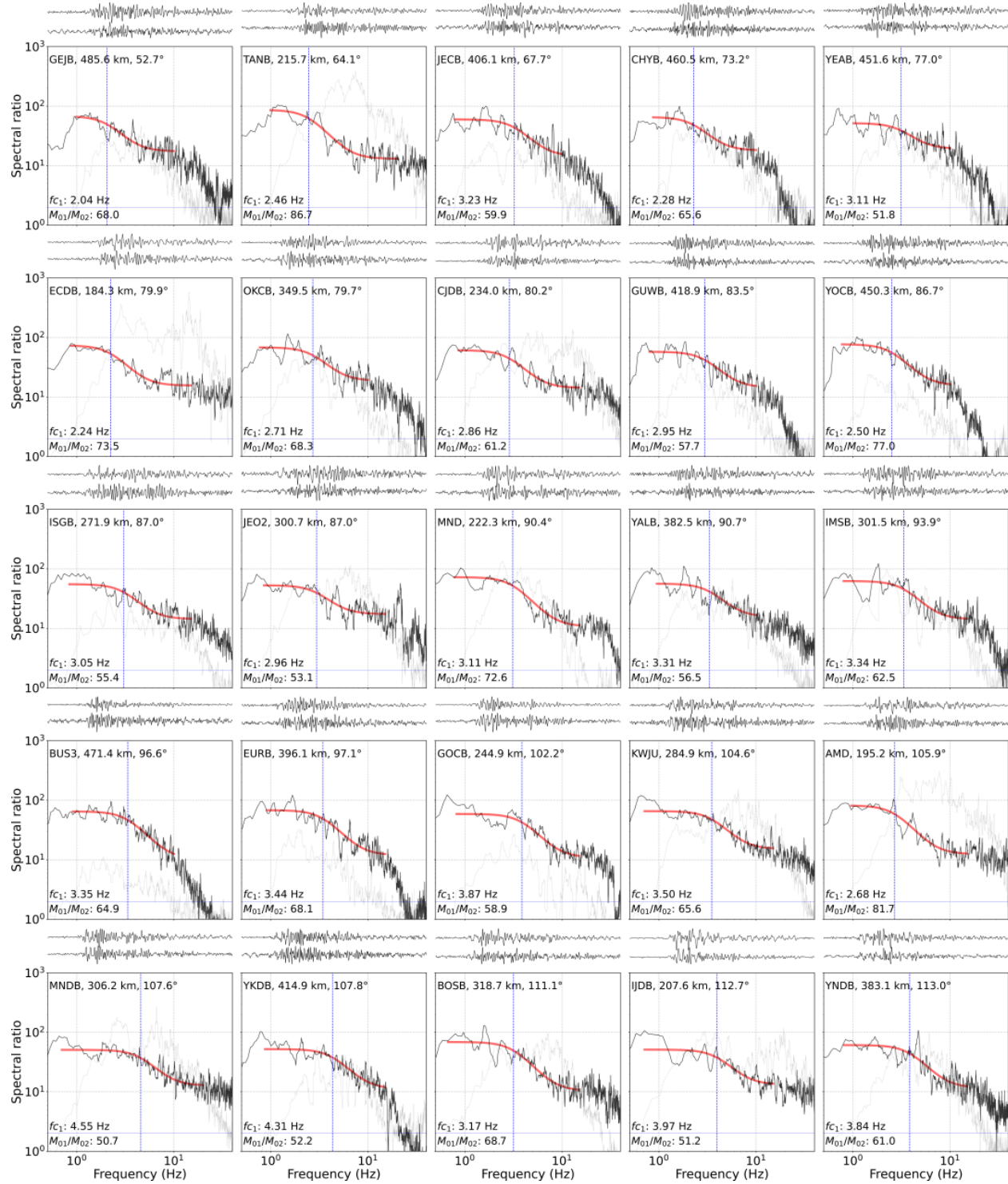


Figure S12. (continued)

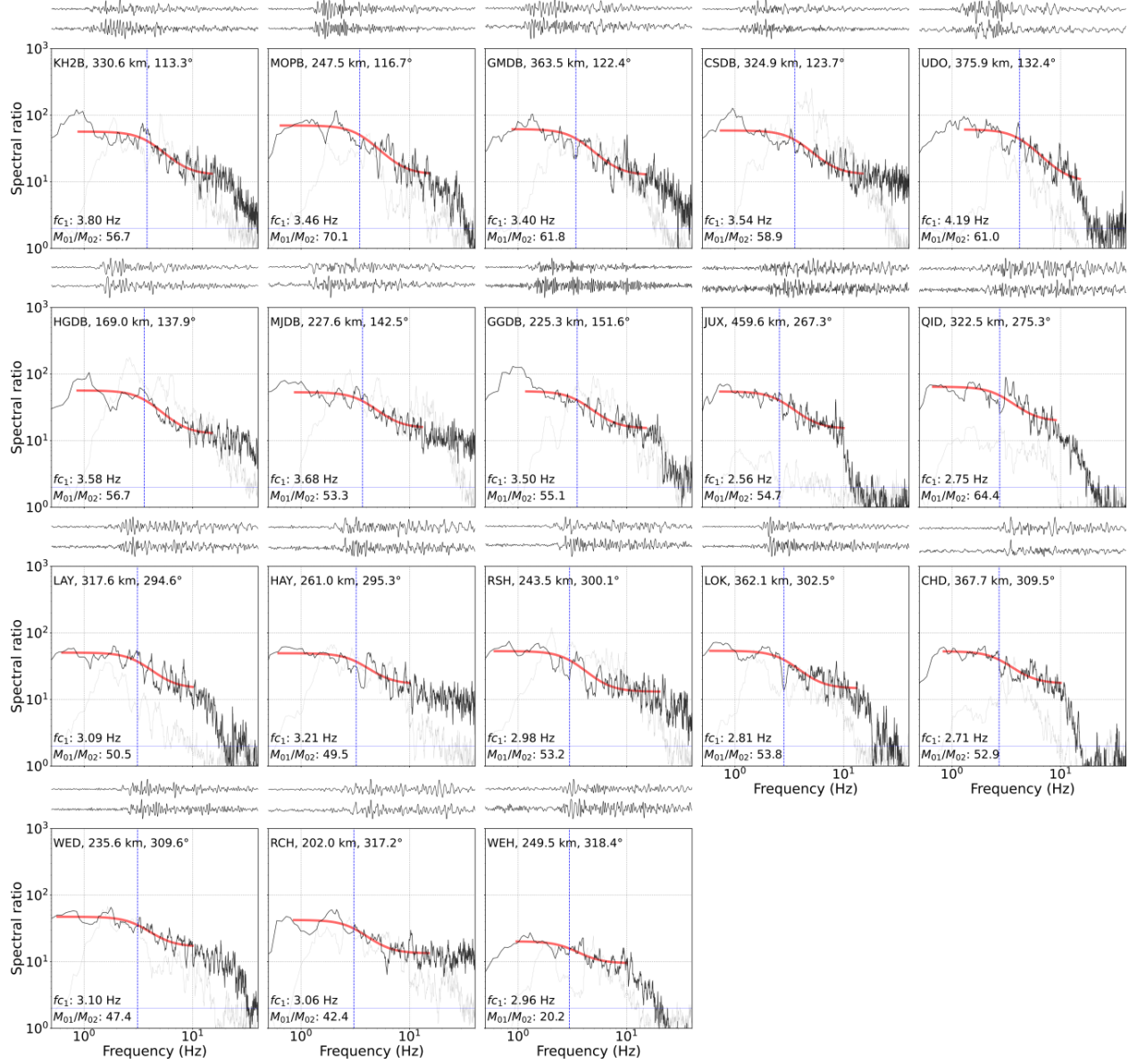


Figure S12. Spectral ratio between target (event 1) and EGF (event 5). Black and red solid lines represent observed spectrum and modeled one from Boatwright (1980) for each station. Waveforms are plotted above each spectrum plot. Blue dotted vertical lines represent determined corner frequency of target and EGF events in each station. Station name, distance, azimuth, corner frequency and moment ratio are specified in each figure.

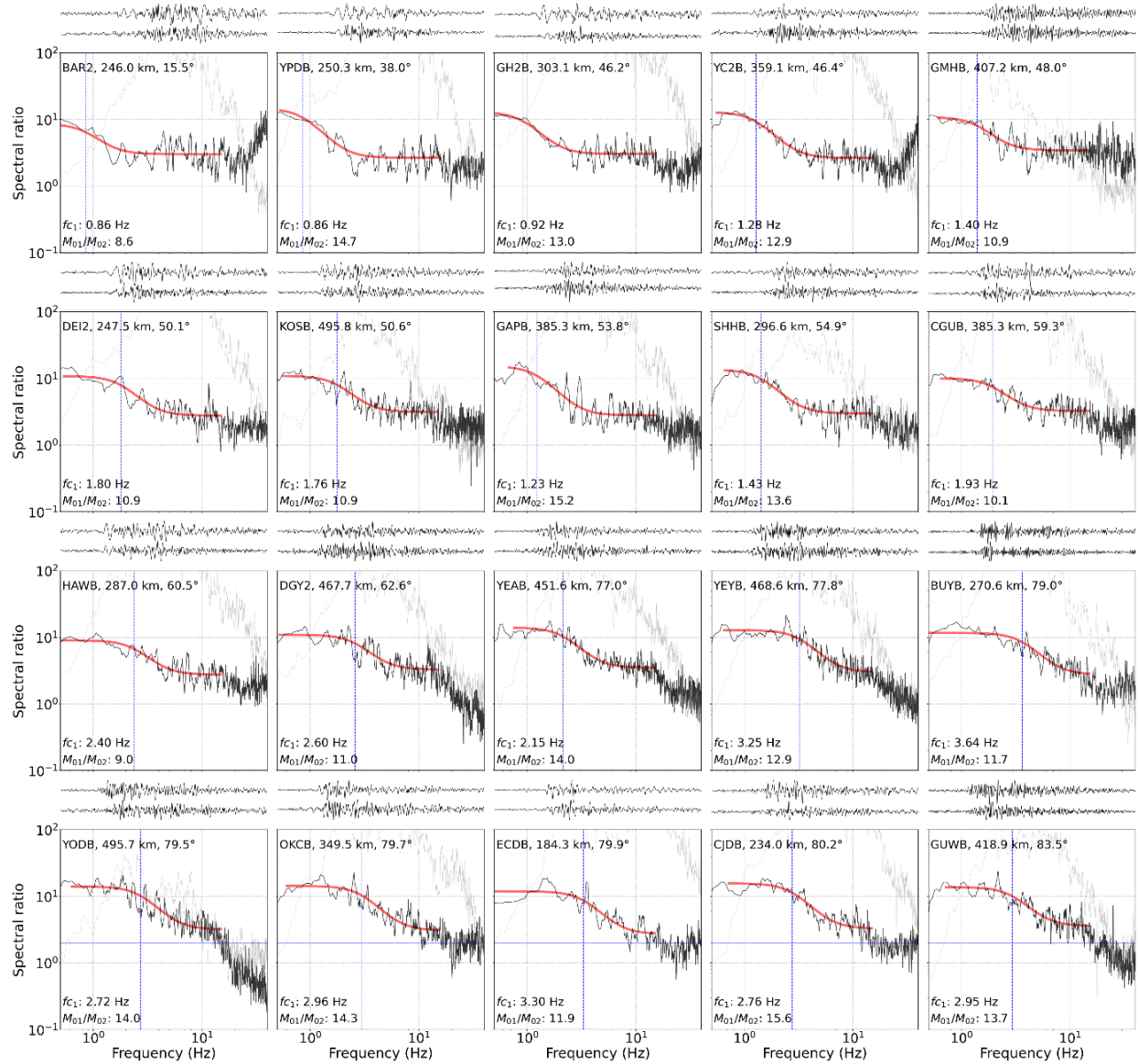


Figure S13 (continued).

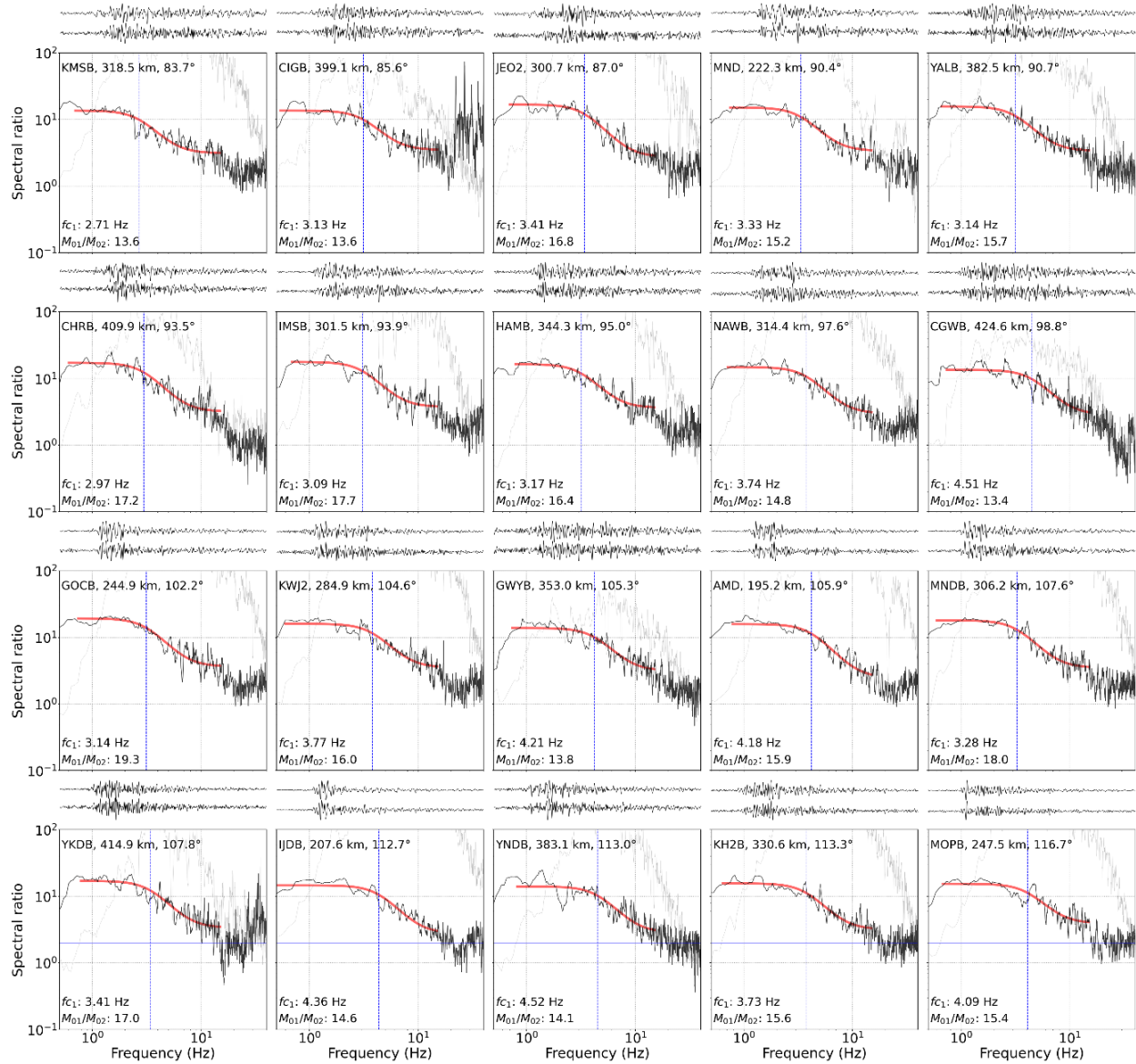


Figure S13. (continued)

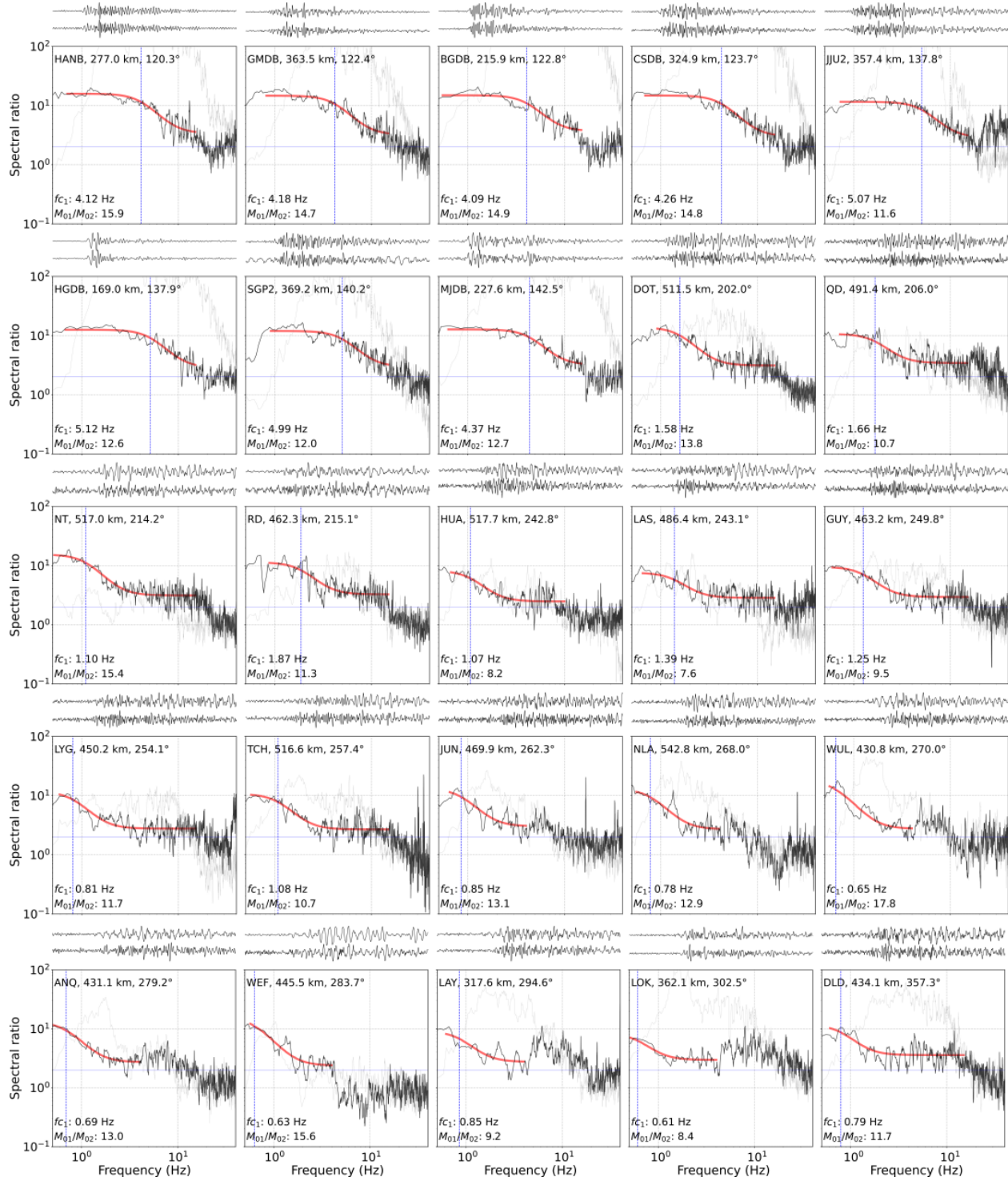


Figure S13. Spectral ratio between target (event 7) and EGF (event 8). Others are the same as Fig. S12.

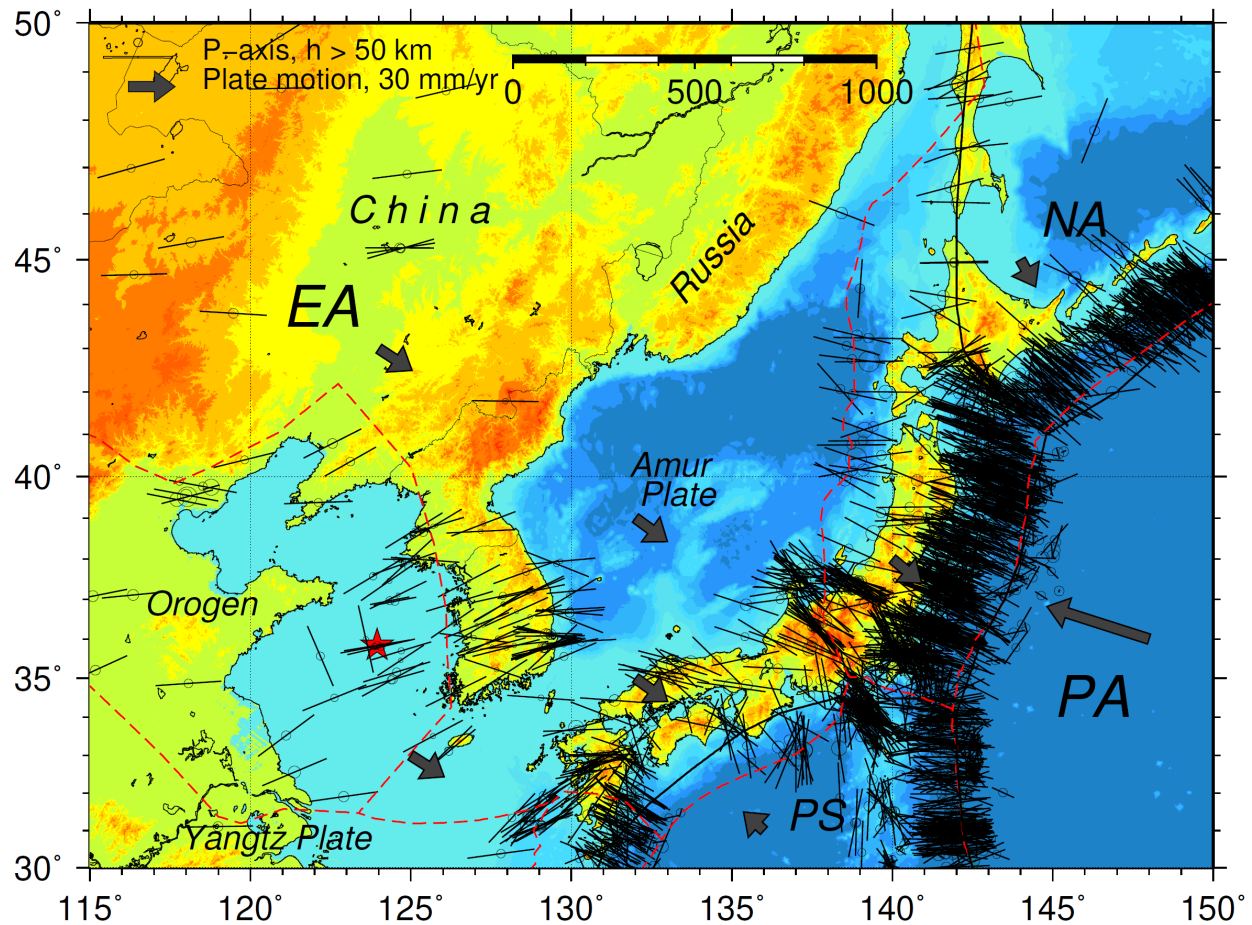


Figure S14. The horizontal projection of the P axis of 2,204 shallow earthquakes (< 70 km) during 1976 – 2023 from the Global Centroid Moment Tensor (GCMT) catalog and 66 earthquakes that occurred in the Korean Peninsula and the Yellow Sea between 1996 and 2023 with known focal mechanisms are plotted. P-axis orientation is shown as a thick bar whose direction is the trend, and the length represents the plunge. The inset bar shows plunge= 0° (horizontal). P-axis orientations of the 18 January and 3 December 2021 Gunsan Basin earthquakes are consistent with those events in the overall Yellow Sea and Korean Peninsula.

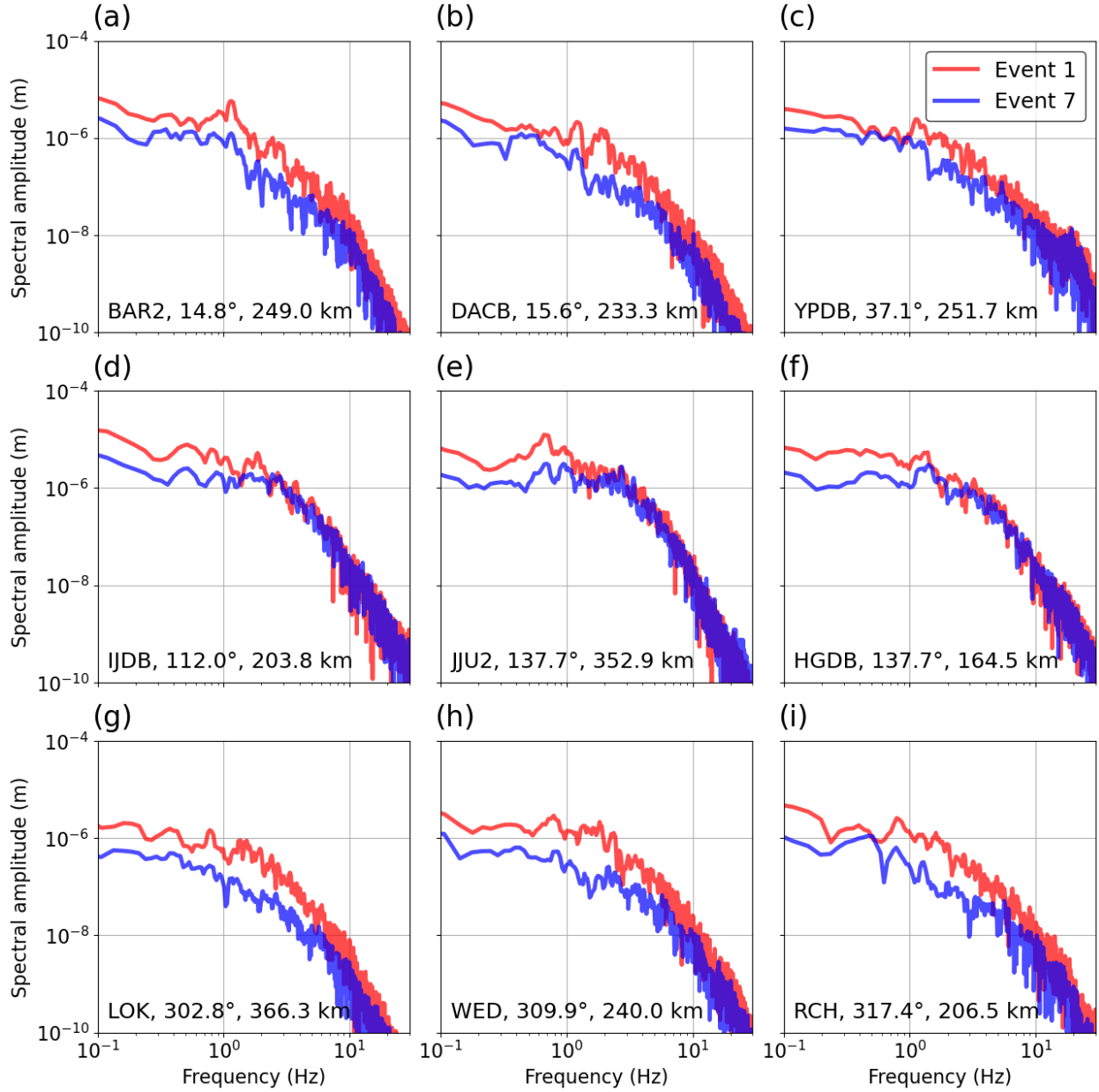


Figure S15. Comparison of observed displacement amplitude spectra of Lg wave of events 1 and 7 at common stations. (a) – (c) Stations in rupture normal direction ($35^\circ \pm 20^\circ$), (d) – (f) stations in rupture direction ($125^\circ \pm 15^\circ$), and (g) – (i) stations in opposite rupture direction ($305^\circ \pm 15^\circ$). Stations are at a distance range from 165–366 km, and station code and azimuth are indicated in each panel. Although the spectra are not corrected for anelastic attenuation, high-frequency contents and fall-off at stations along the presumed rupture direction (d – f) are higher than those in other directions. Notice that spectral amplitudes between 1 and 5 Hz from the event 7 at stations in the opposite direction of rupture (g – i) show lower amplitudes than those from the event 1.

Table S1. Earthquake Parameters of the 2021 Offshore Gunsan Earthquake Sequences

Events reported by KMA

ID	Date	Time (UTC)	Lat. (°N)	Long. (°E)	H (km)	M_L	M_w	Imax
1	2021-01-18	18:21:28	35.79	123.97	12	4.6	4.7	II
2	2021-01-19	13:58:32	35.76	123.97	23	1.9		
3	2021-01-21	21:01:48	35.76	123.96	12	3.2		
4	2021-01-29	13:34:55	35.80	123.99	15	2.6		
5	2021-02-04	01:56:22	35.75	124.02	17	2.9		
6	2021-03-09	17:56:24	35.77	123.97	10	1.9		
7	2021-12-03	12:08:22	35.81	123.88	17	4.5	4.2	II
8	2021-12-03	15:18:09	35.80	124.02	-	3.4		
9	2021-12-04	00:30:18	35.77	124.01	-	2.2		

Events reported by ISC*

ID	Date	Time (UTC)	Lat. (°N)	Long. (°E)	H (km)	Magnitude	Agency
1	2021-01-18	18:21:28.34	35.825	124.060	10.0	mb 4.3	ISC*
3	2021-01-21	21:01:49.29	36.017	123.916	15.8	M_L 3.4	KEA [†]
4	2021-01-29	13:34:59.50	36.017	123.939	23.0	M_L 2.9	KEA [†]
5	2021-02-04	01:56:19.22	36.017	123.826	15.9	M_L 3.3	KEA [†]
7	2021-12-03	12:08:21.18	35.686	124.042	0.0	mb 3.6	IDC [‡]
8	2021-12-03	15:18:16.86	36.267	124.257	1.0	M_L 3.5	KEA [†]

* ISC (International Seismological Centre),

[†] KEA (Korea Earthquake Administration, DPRK),

[‡] IDC (International Data Center, CTBTO)

References

- Bird, P. (2003). An updated digital model of plate boundaries. *G-cubed*, **4**, no. 3.
- Boatwright, J. (1980). A spectral theory for circular seismic sources; simple estimates of source dimension, dynamic stress drop, and radiated seismic energy. *Bull. Seismol. Soc. Am.* **70**, no. 1, 1-27.
- Kennett, B. L. N., and Engdahl, E. R. (1991). Travel times for global earthquake location and phase identification. *Geophys. J. Int.* **105**, no. 2, 429-465.
- Kennett, B. L.N., Engdahl, E. R., and Buland, R. (1995). Constraints on seismic velocities in the Earth from traveltimes. *Geophys. J. Int.* **122**, no. 1, 108-124.
- Klein, F. W. (2002). User's guide to HYPOINVERSE-2000, a Fortran program to solve for earthquake locations and magnitudes (No. 2002-171). *US Geological Survey*.
- Waldhauser, F. (2001). hypoDD--A program to compute double-difference hypocenter locations.
- Waldhauser, F. and Ellsworth, W. L. (2000). A double-difference earthquake location algorithm: Method and application to the northern Hayward fault, California. *Bull. Seismol. Soc. Am.* **90**, no. 6.